Conceptual Assessment of Lightbridge Fuel™ Post-CHF Performance

Birol Aktas*

Lightbridge Corporation, Reston, VA

doi.org/10.13182/TOPFUEL25-48597

ABSTRACT

Lightbridge Fuel™, which is a U-Zr alloy fuel in a helically twisted and multi-lobed geometry, consisting of approximately 50 weight percent of each material, can help the nuclear industry leverage "time-at-temperature" effectively. Time-at-temperature is a strategy that defines a time vs. temperature envelope based on an allowable recovery of cladding irradiation hardening and α-β phase transition in zirconium cladding, rather than maintaining margins for deteriorating heat transfer conditions during plant events as stipulated in current fuel licensing requirements. This strategy has been recently embraced by the nuclear industry after investing in accident tolerant fuel technologies. There are, however, challenges in implementing this strategy, stemming from the severity of fuel cladding temperatures experienced during some plant events of interest to pressurized water reactors, particularly the instantaneous seizure of a reactor coolant pump rotor (locked rotor) event. A conceptual assessment of fuel temperatures experienced by Lightbridge fuel during this event is provided here, along with background information to articulate the strengths of the Lightbridge fuel design in the context of the time-at-temperature strategy. The assessment also addresses a potential concern about the current lack of thermophysical properties for irradiated U-Zr alloys of Lightbridge fuel. Based on the operating experience and qualification data for Lightbridge's metallurgically bonded, monolithic U-Zr alloy fuel form, it is concluded that fuel temperatures experienced by Lightbridge fuel during the locked rotor event are well below any known temperature limit.

Keywords: U-Zr alloy fuel, time-at-temperature, locked rotor, DNB, post-CHF

1. INTRODUCTION

There has been a growing recognition that the current licensing approach to prevent fuel and cladding overheating during normal operations and Anticipated Operational Occurrences (AOOs) is excessively conservative. It has also been recognized that "the excessive conservatism entails a significant economic burden on the industry without any proportional enhancement in safety" [1]. Hence the activities undertaken by the U.S. nuclear industry toward replacing the thermal hydraulic design criteria, currently prescribed in Section 4.4 of the U.S. NRC's Standard Review Plan [2], in favor of new cladding material-properties-based criteria as fuel design limits. Rather than insisting that an adequate margin to the departure from nucleate boiling (DNB) in PWRs and the liquid film dryout in BWRs be maintained to prevent fuel and cladding overheating, this new approach will allow a time vs. temperature envelope defined by an allowable recovery of cladding irradiation hardening and α-β phase transition in zirconium cladding. It is worth remembering that the approach, widely known as "time-at-temperature" has been considered and implemented in other countries and has fueled extensive research in reactor thermal hydraulics known as

* baktas@ltbridge.com

"post-CHF" at conditions relevant to both BWR and PWR operations [3]. The approach caught the U.S. nuclear industry's attention only after it invested in Accident Tolerant Fuel (ATF) technologies, spurred by the Fukushima Daiichi accident, and realized that these fuels could "operate in post-DNB and post-dryout conditions without requiring their replacement" [4].

Operating with a time-at-temperature envelope that allows an option for return-to-service after AOOs can "be used to greatly improve plant operational flexibility, allow faster startup times from outages, or justify increased reactor thermal power" [4]. The return-to-service option is thus seen as a crucial factor when forecasting the benefits of the time-at-temperature approach. This option, however, seems less likely for PWRs. The issue stems from the severity of post-CHF conditions in PWRs, during which cladding temperatures quickly exceed the α-β phase transition in zirconium cladding [5]. The severity of post-CHF conditions affects the prospect of return-to-service through two particularly important phenomena: the recovery of cladding irradiation hardening, and cladding creep-down and collapse [1]. These phenomena are not relevant to the monolithic design of U-Zr alloy fuel, which features a metallurgical bond between the Zr alloy cladding and the metallic fuel core. Thus, Lightbridge's metallic U-Zr alloy fuel can help the nuclear industry leverage time-at-temperature more effectively.

Furthermore, the higher thermal conductivity and diffusivity of zirconium-rich U-Zr alloys, relative to the properties of UO_2, provide a distinct advantage. The former translates to lower fuel temperatures, and the latter produces a faster thermal response. This study investigates the effects of U-Zr alloy thermophysical properties on post-CHF heat transfer as separate effects. In this study, the Lightbridge fuel was modeled as having the cylindrical geometry and cladding and pellet dimensions of a PWR 17x17 type fuel rod, rather than the helical cruciform shape for which Lightbridge fuel is known in order to focus on the effect of thermophysical properties. The post-CHF heat transfer is studied at a hot spot, postulated using the description of an instantaneous seizure of a reactor coolant pump rotor (locked rotor) event. The aim is to quantify the potential impact of thermal conductivity and diffusivity on the application of time-at-temperature in future core designs with Lightbridge fuel.

First, a brief background on Lightbridge fuel is shared, including information that supports its potential with the time-at-temperature strategy. A survey of the thermophysical properties of zirconium-rich U-Zr fuel alloys is followed by a description of the fuel and cladding overheating exercise chosen for this study. Next, a hot spot analysis, which focuses on the effects of thermophysical properties on post-CHF fuel temperatures, is presented. The results support the conclusion that Lightbridge's metallic U-Zr alloy fuel can benefit to the fullest from implementing a time-at-temperature strategy.

2. LIGHTBRIDGE FUEL

Lightbridge fuel, a four-lobed version of which is shown in Figure 1, is an all-metallic U-Zr alloy fuel with a helically twisted and multi-lobed geometry, composed of approximately 50 weight percent (wt%) of each material (intermetallic δ-UZr_2 phase). The helical twist creates contact points across self-spacing planes, allowing the design of fuel assemblies without spacer elements. This metallurgically bonded, monolithic fuel form reduces the importance of cladding, both as a fission-product barrier during design basis accidents (DBAs) and for structural support in their aftermath. This, in turn, alleviates the significance of any impact on cladding material properties from exposures to high temperatures during AOOs and DBAs.

A three-lobed version of Lightbridge fuel has proven capable of supporting power uprates and extended fuel cycles in Russian design Water-Water Energetic Reactors (VVERs) [6, 7]. The technical feasibility in VVERs was supported by dedicated irradiation testing and thermal-hydraulic experiments, performed at Kurchatov Institute. These tests confirmed key design features such as the integrity of the metallurgical bond between cladding and fuel under accident conditions, the microstructure stability of zirconium rich U-Zr alloy fuels at elevated temperatures, the pressure drop characteristics of helically twisted fuel geometry, and its critical heat flux performance. Lightbridge is currently undertaking a development program to demonstrate comparable fuel performance for the U.S. domestic PWRs and BWRs.

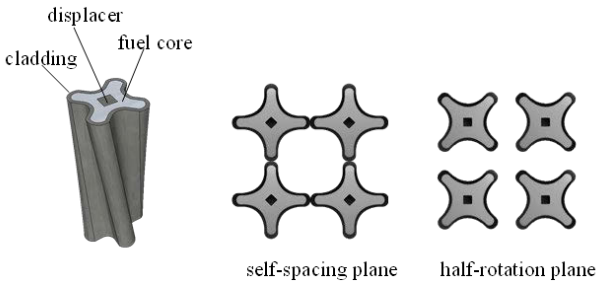

Figure 1. Helical cruciform fuel geometry.

2.1. Icebreaker Fuel Experience

The design of Lightbridge fuel for use in commercial light water reactors (LWRs) was adapted from an earlier fuel that was used for many decades in icebreaker reactors [7]. The icebreaker fuel design bases included the operation of all-metallic U-Zr alloy fuels under rapidly changing power levels, subject to fluctuating coolant pressure and temperatures, at peak linear rates exceeding 22 kW/ft, and 1.5 g/cc (est. 45 %at) burnup in U-60Zr fuel accumulated over 3.5 years at full power. Other highlights of icebreaker experience included the operation of failed fuel rods, which had gone undetected for several months without any sign of coolant contamination. Post-irradiation examinations revealed that fuel alloy oxides filled the defects formed in the cladding and fuel, mitigating the release of fission products from the rods that had failed during a rapid blowdown due to a pipe break and subsequent loss of coolant flow – the reactor operation resumed after the broken loop was repaired with no replacement fuel.

The material properties and mechanical performance of U-Zr alloy fuels observed during the icebreaker fuel development program add to the appeal of Lightbridge fuel for operating with a time-at-temperature envelope that allows return-to-service after AOOs. The following observations, made under very extreme circumstances created by prolonged exposures to loss-of-flow scenarios and at power densities that far exceeded typical LWR power levels, suggest a robust expected performance by Lightbridge fuel as a fission product barrier capable of supporting extended fuel cycles and power uprates.

1. The operation of metallurgically bonded fuel without failure until near full fuel burnup.
2. The ability of the metallurgical bond to withstand extremely high energy deposition during RIAs – concurrent straining of the bonded cladding and fuel core.
3. No impact from zirconium hydrates on the performance of bonded cladding.
4. The fission gas bubble formation threshold well above nominal LWR temperatures.
5. Stable microstructures of U-Zr alloy fuel even after annealing at temperatures above the phase transition boundary for several days.
6. Swelling consistent with anticipated gas bubble growth, open pore formation, and fission product accumulation.

2.2. Improved Thermal Hydraulic Performance

The helical, multi-lobed geometry of Lightbridge fuel further improves fuel rod heat transfer by increasing the heated surface area and promoting turbulent mixing. Its helically twisted fuel rod geometry has proven to improve thermal-hydraulic performance in its application of the three-lobed design for VVERs, supported by experimental CHF and pressure loss data measured in single-rod, seven-rod, and 19-rod test assemblies [8]. The four-lobed version, also known as helical cruciform fuel (HCF), continues to receive attention, as is evident in the published research [9-14]. These publications cover a wide range of issues considered in the thermal hydraulic evaluations of U-Zr alloy HCF rods, with conclusions that suggest a

strong correlation between the performance of the three- and four-lobed fuel rod geometries. Some highlights include the following:

1. Decreasing CHF performance under DNB conditions with increasing wall superheat (relative to that of a standard PWR fuel geometry).
2. Increased rod surface area for heat transfer, which reduces the heat flux and fuel temperatures.
3. Non-uniform circumferential heat flux, with higher heat flux away from the lobes near the "valleys".
4. Higher frictional pressure losses (relative to that of a standard PWR fuel geometry).
5. Sweeping cross flows and turbulent heat transfer promoted by the lobes.

The focus of published research, with the exception of Conboy's dissertation [9], did not include the application of helical, multi-lobed fuel at BWR conditions, which would require understanding the effect of geometry on entrainment and deposition in annular two-phase flow. The development program at Lightbridge is aiming to characterize fuel rod heat transfer at conditions relevant to reload licensing, including those relevant to BWRs. An accurate description of core cooling hydraulics in reactors with Lightbridge fuel will require considering the effects of helical cruciform geometry on coolant flow and fuel rod heat transfer at confidence levels appropriate for reload licensing. Doing so is necessary to develop a time vs. temperature envelope for Lightbridge fuel that allows return-to-service after AOOs, with adequate margins to material-properties-based criteria specified as fuel design limits.

3. U-ZR ALLOY THERMOPHYSICAL PROPERTIES

The data on thermophysical properties of U-Zr alloys can be found in metallic fuel handbooks dating back to the early 1950s[1] as well as in more recently published versions [15-17]. There is, however, greater emphasis on uranium-rich U-Zr alloys in the historical data as those compositions have higher heavy metal density and thermal conductivity, which suited the needs of sodium fast reactor designs at the time. Unlike fast reactors, which can accommodate significant irradiation-induced growth by operating low smear density metal fuel rods at relatively high temperatures, the preferred U-Zr composition for thermal reactors is the heat-treated, zirconium-rich U-Zr alloys that exhibit intermetallic hexagonal δ-phase, due to their resistance to irradiation-induced growth. Such is the design of Lightbridge fuel.

The literature on thermophysical properties of zirconium-rich U-Zr alloys documents a strong dependence on the fuel's temperature and composition, burnup, porosity, and irradiation conditions [18, 19]. The thermal conductivity of U-50Zr consists of electronic and phonon conductivity [20]. It has been reported in recently published articles that "the δ-phase exhibits significant thermal anisotropy" [21], and that "the connections among irradiation, nanostructure, phonons, and thermal conductivity remain unknown" [22]. Until qualification data from post-irradiation examinations of irradiated fuel become available, understanding the effect of thermophysical properties is important for conceptual and preliminary design studies. The development program at Lightbridge will accordingly identify these important phenomena and characterize the bulk thermophysical properties of Lightbridge Fuel using appropriate methods.

Two sources, selected for this study, report the thermophysical properties for the 50 and 60 wt% U-Zr alloy. The first source by Beausoleil et al.[23] reports the thermophysical properties of unirradiated U-50Zr alloy samples, fabricated via arc-melting and drop casting using the legacy EBR-II depleted uranium (DU) feedstock. The second source by Gaiduchenko et al.[19, 24] report the thermophysical properties of unirradiated and irradiated U-60Zr fuel samples. The irradiated samples had the burnup levels of 11.9, 17.8, and 26.8 at%. Although the second source did not characterize the source of U-60Zr samples, it is deduced by association that these samples had originated from the Russian icebreaker fuel development program.

[1] It was also noted that "the cladding of zirconium-uranium alloys with Zircaloy [had] proven to be very successful, with good metallurgical bonds being obtained."

The thermal conductivity and diffusivity of U-Zr alloys reported in these two sources are shown in Figure 2 – the properties of UO_2 fuel at 2.6 at% are included as a reference.

Takahashi et al. reported the thermophysical properties of U-Zr alloys in the 10 to 80 wt% range zirconium content [18]. Their data show that thermal conductivity becomes minimum at ~50 wt% where the intermetallic δ-phase forms. The same data also indicate only minor differences in the thermal properties of U-Zr alloy within the 30 to 80 wt% zirconium range. Therefore, the thermodynamic properties of the irradiated U-60Zr samples by Gaiduchenko et al. offer valuable guidance until data for irradiated U-50Zr become available. A thorough understanding of the differences in the properties of U-Zr alloys shown in Figure 2 is beyond the scope of this study. However, it suffices to say that the development program at Lightbridge will consider the subtleties in the characterization of these bulk thermophysical properties.

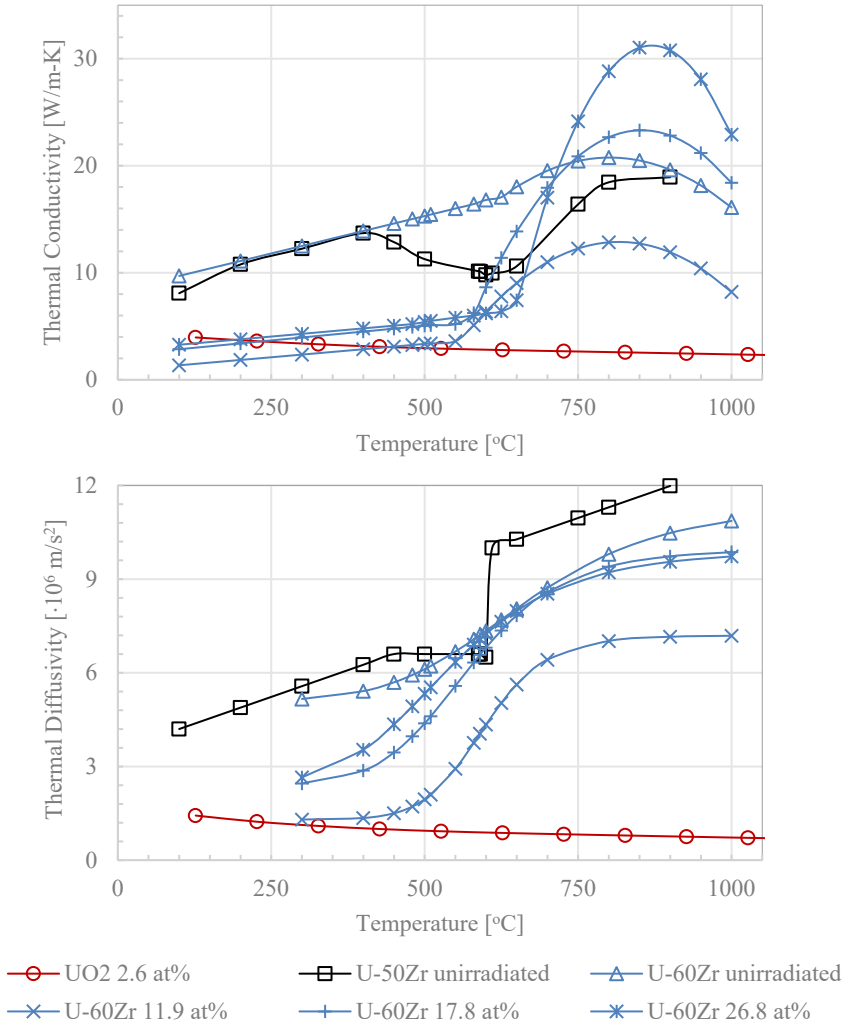

Figure 2. Thermal conductivity and diffusivity of U-Zr fuel alloys.

4. FUEL AND CLADDING OVERHEATING

The locked rotor event, selected for the purpose of this study, focuses on DNB in PWRs. This event, classified as a limiting fault incident, can be summarized as a rapid flow reduction through the affected

loop, terminated by a reactor trip on a low flow signal. Inadequate transfer of the stored heat in fuel rods, due to the rapid loss of coolant flow, precipitates the onset of DNB.

The heat transfer from PWR fuel rods to the coolant can range from single-phase forced convection to subcooled nucleate boiling at typical operating pressures of 15-16 MPa. The formation, growth, and detachment of vapor bubbles enhance the heat transfer in subcooled nucleate boiling regime. DNB can be characterized simply as the inability of liquid water to reflood the nucleation sites due to the overcrowding of fuel rod surface by vapor bubbles, which is a hydrodynamically driven phenomenon of counter current flow limitation between the liquid and vapor phases, commonly referred to as the vapor blanketing. The onset of DNB results in a sudden drop of heat transfer, which is identified as a critical point prior to the temperature excursion on a heat flux vs. wall temperature boiling curve – hence, the origin of term "critical heat flux."

The local conditions for the purpose of this study, which precipitate the onset of DNB, during this event were ad hoc calibrated to the locked rotor event description in Section 15.3.3 of Byron/Braidwood Nuclear Stations Updated Final Safety Analysis Report (UFSAR) [25]. Specifically, Figures 15.3-5 and 15.3-6, which depict reactor power, coolant system pressure, and core coolant flow as the fractions of initial values (Figure 3), were used in tandem with the core design parameters (Table I) from Table 4.1-1 of the UFSAR [26]. Table II and Figure 3 present the initial and transient boundary conditions for a postulated hot rod, derived from the UFSAR data.

Table I. PWR 17x17 type fuel rod geometry.

Outside Diameter, mm (in.)	9.1 (0.360)
Diametral Gap, mm (in.)	0.157 (0.0062)
Cladding Thickness, mm (in.)	0.572 (0.0225)
Cladding Material	Zircaloy-4/ ZIRLO
UO_2 Density	95 % of TD
Pellet Diameter, mm (in.)	7.8 (0.3088)

Table II. PWR single rod initial and boundary conditions.

Pressure, MPa (psia)	15.7 (2270)
Power, kW (BTU/hr)	120.9 (412600)
Mass Flux, kg/s-m^2 (Mlb$_m$/hr-ft^2)	2848 (2.1)
Inlet Temperature, ºC (F)	290.7 (555.2)

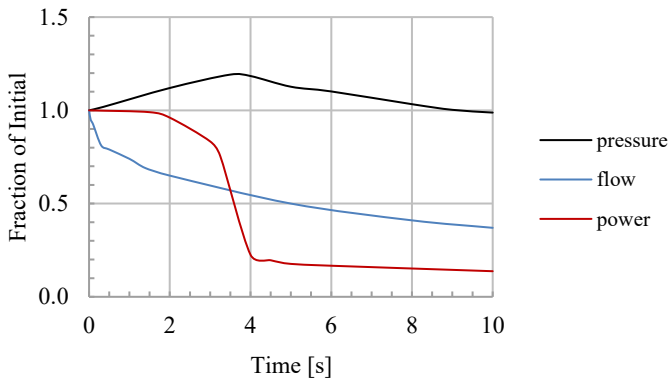

Figure 3. Single reactor coolant pump locked rotor.

5. HOT SPOT ANALYSIS

TRACE, the U.S. NRC's reactor safety analysis code, was used in this study to perform the hot spot analysis exercise. Its built-in material properties for UO_2 and zircaloy cladding as well as the post-CHF heat transfer models for transition boiling and film boiling were leveraged throughout the study. A brief description of heat transfer modeling is provided here at a level of detail sufficient to describe the method of analysis. The reader is referred to Chapters 6 and 8 of the TRACE Theory Manual for detailed descriptions of the fuel rod and wall heat transfer models [27].

The use of separate mass, energy, and momentum conservation equations in TRACE for the liquid and gas fields enables a phenomenological construction of post-CHF wall heat transfer. These equations contain the following terms, which represent heat transfer from the wall to the liquid, to the boiling liquid, and to the gas, respectively:

$$q''_{wl} = h_{wl} \cdot (T_w - T_l) \quad (1)$$

$$q''_{wsat} = h_{wsat} \cdot (T_w - T_{sat}) \quad (2)$$

$$q''_{wg} = h_{wg} \cdot (T_w - T_g) \quad (3)$$

where h_{wl} is the heat transfer coefficient associated with heating of the liquid, h_{wsat} is the heat transfer coefficient for direct boiling of the liquid, h_{wg} is the wall-to-gas heat transfer coefficient.

Nucleate boiling is initiated if the wall superheat is sufficient ($T_w > T_{ONB}$) to activate nucleation sites present on the wall surface. If the wall superheat exceeds a critical temperature at which the CHF occurs ($T_w > T_{CHF}$), the liquid-wall contact becomes intermittent (transition boiling) or non-existent (film boiling). Should the wall surface be too hot for liquid to maintain contact ($T_w > T_{MIN}$), film boiling is initiated, characterized by an inverted annular flow topology.

For the onset of DNB, Groeneveld's 2006 AECL CHF table was used [28]. Noting that an accurate simulation of DNB in modern PWR 17x17 fuel assemblies requires empirical correlations based on fuel-specific CHF data and design-specific thermal-hydraulic models, the hydrodynamically controlled phenomena at the rod surface (i.e., DNB) are reduced to a time-dependent pair of heat transfer coefficient and coolant temperature when studying the effects of thermophysical properties on post-CHF fuel temperatures.

The method of analysis includes the following steps.

1. A single-subchannel analysis, consisting of a single UO_2 fuel rod, was developed using the initial and transient boundary conditions for the locked rotor event. A mid-flat axial power shape, with 1.28 axial peaking in the flat region and a corresponding peak linear heat rate of 37.3 kW/m (12.7 kW/ft), was used. The UO_2 thermophysical properties were evaluated at 25 MWd/kgU (2.6 at%) burnup. The gap size was reduced to four times the cladding surface roughness, which was considered appropriate for this assumed burnup level. At steady state, a minimum CHF ratio of 1.52 was predicted at 2.82 m elevation from the bottom of the active fuel, with a heat flux of 1.3 MW/m^2 (corresponding to 11.4 kW/ft). During the transient, the onset of DNB was observed[2] at the same elevation after the local mass flux dropped below 2000 kg/s-m^2 as the heat flux remained at its initial value of 1.3 MW/m^2. This single-subchannel analysis was repeated for U-50Zr alloy

[2] Fuel design-specific correlations and models from a fuel vendor, developed using prototypic test assembly pressure drop and temperature data and when exercised in a subchannel analysis model, are likely to predict the onset of DNB at a lower mass flux threshold and a higher thermodynamic quality.

fuel placed inside a matching rod geometry, except there was no fuel cladding gap. Figure 4 shows the local conditions at the elevation where the onset of DNB is first observed.

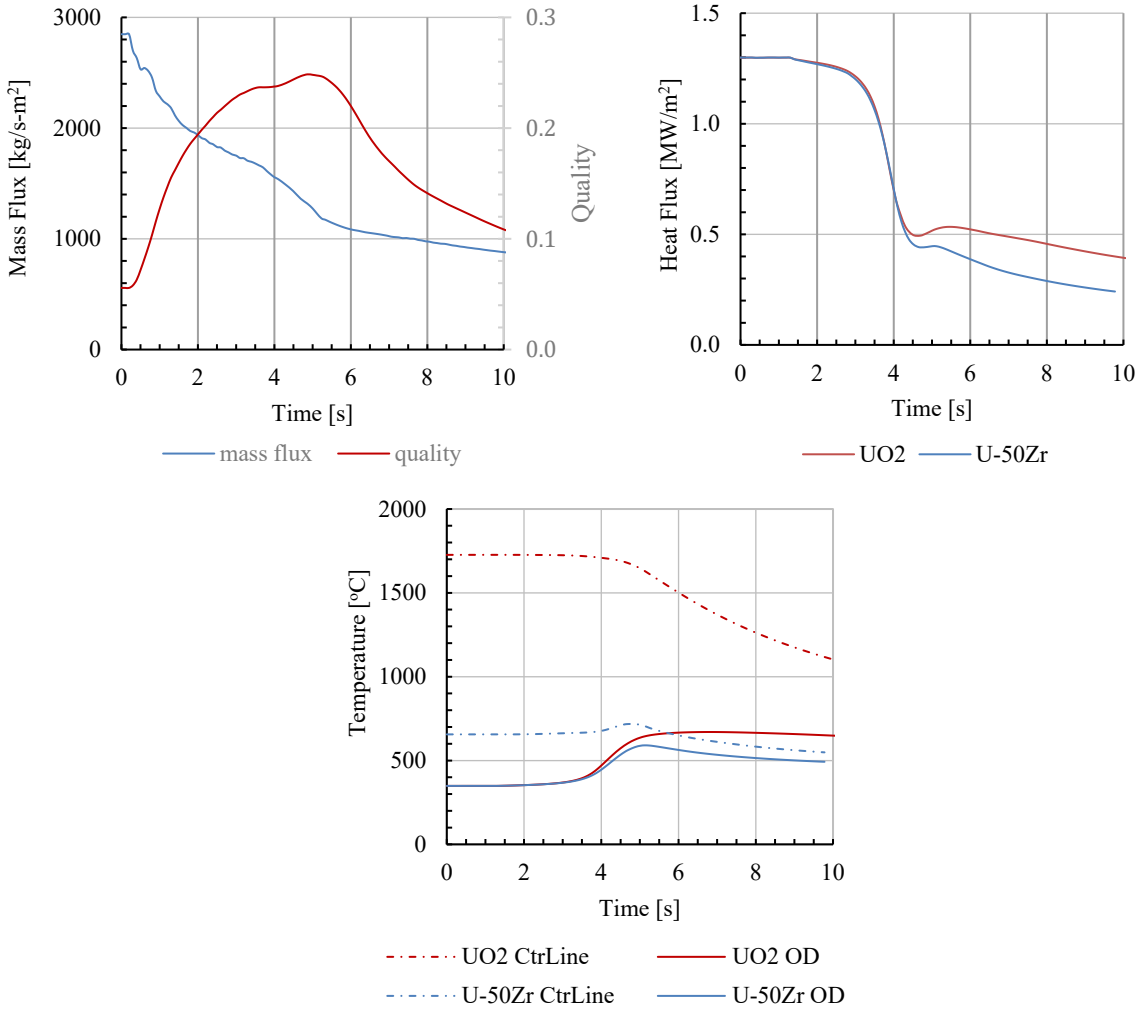

Figure 4. Local conditions at 2.82 m elevation.

2. A table of time-dependent heat transfer coefficient and coolant temperature pairs were defined at the DNB location as follows:

$$h_w = h_{wl} + h_{wsat} + h_{wg} \tag{4}$$

$$\Delta T_w = (h_{wl} \cdot \Delta T_{wl} + h_{wsat} \cdot \Delta T_{wsat} + h_{wg} \cdot \Delta T_{wg})/h_w \tag{5}$$

$$T_c = T_w - \Delta T_w \tag{6}$$

Figure 5 shows the heat transfer coefficients from the wall to the liquid, to the boiling liquid, and to the gas, along with the time-dependent pairs of an overall wall heat transfer coefficient and a coolant temperature, all determined at this step.

In Figure 5, the first inflection point of the boiling heat transfer coefficient (h_{wsat}) at 2 seconds is indicative of an intermittent liquid-wall contact after the wall temperature exceeds a critical value at which the CHF occurs, i.e., transition boiling. The second inflection point at 5 seconds happens

when the rod surface is too hot for liquid to maintain contact and heat transfer from the wall to the gas (h_{wg}) dominates, i.e., film boiling. The surface temperatures at the rod outer diameter (OD), shown for both UO_2 and U-50Zr fuels in Figure 4, reach their peak values within one second after film boiling is initiated.

These results are based on phenomenological models, implemented in TRACE with the intent to simulate the mean behavior of a system-level response to such events. This breakdown of rod surface heat transfer (from the rod surface to the liquid, to the boiling liquid, and to the gas) may therefore not be an accurate picture of reality. That level of consistency is, nevertheless, not required, as the rapid rise of cladding temperature under similar mass and heat flux conditions can be corroborated with publicly available experimental data [29].

The local conditions where DNB is observed are controlled hydrodynamically and independent of the fuel type before film boiling is initiated. As such, post-CHF heat transfer can be simulated at a hot spot by simply imposing a wall heat transfer boundary condition to study the effects of fuel thermophysical properties on post-CHF heat transfer as separate effects.

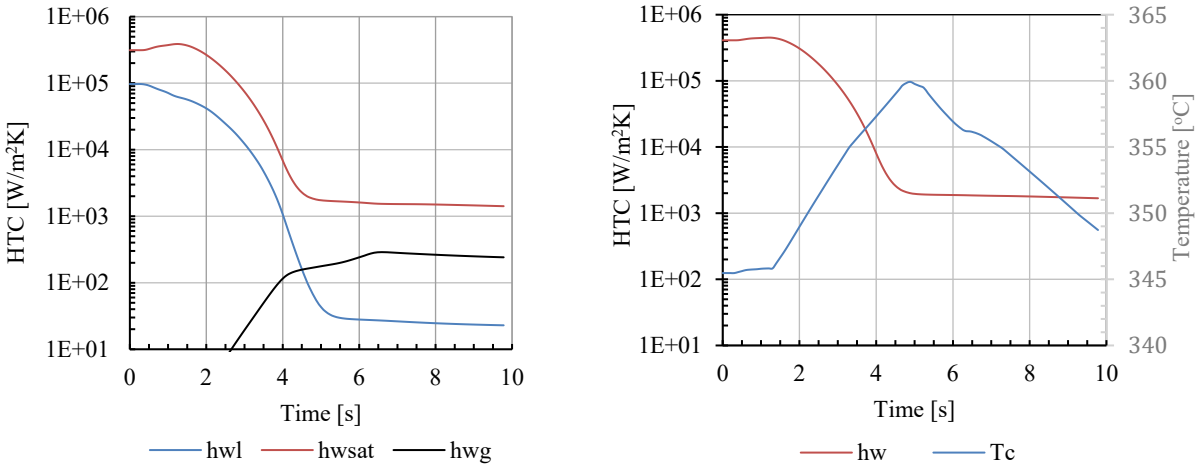

Figure 5. Rod surface heat transfer.

3. A radial heat conduction problem was set up using TRACE, with the time-dependent wall heat transfer boundary condition shown in Figure 5, to predict transient fuel temperatures in unirradiated U-50Zr, unirradiated U-60Zr, and U-60Zr at 11.9, 17.8, and 26.8 at% burnup. This conduction problem was solved repeatedly for linear heat rates iterated from 37.3 kW/m (11.4 kW/ft) to 140% of this initial value (15.9 kW/ft), in increments of 10%. Transient fuel temperatures for UO_2 at 2.6 at% burnup were also evaluated and presented as a reference. The thermal conductivity and diffusivity of U-Zr alloys and UO_2 shown in Figure 2, along with the temperature-dependent density for these fuel materials from the same references (not shown here), were used in the analysis.

   Figure 6 contains two plots showing the fuel centerline temperatures (T_{CL}) and the peak cladding temperature (T_{cladID}) recorded during the transient at each 10% power increment. The peak centerline temperature is the initial temperature, which drops after the reactor trip. The minimum film boiling temperature (T_{MIN}) and the cladding temperature for U-Zr alloy fuels (T_{cladID} at 0s) are also shown as a reference. Although not shown in the figure, the cladding temperature at 0s for UO_2 fuel is slightly higher (~10°C at 15.9 kW/ft).

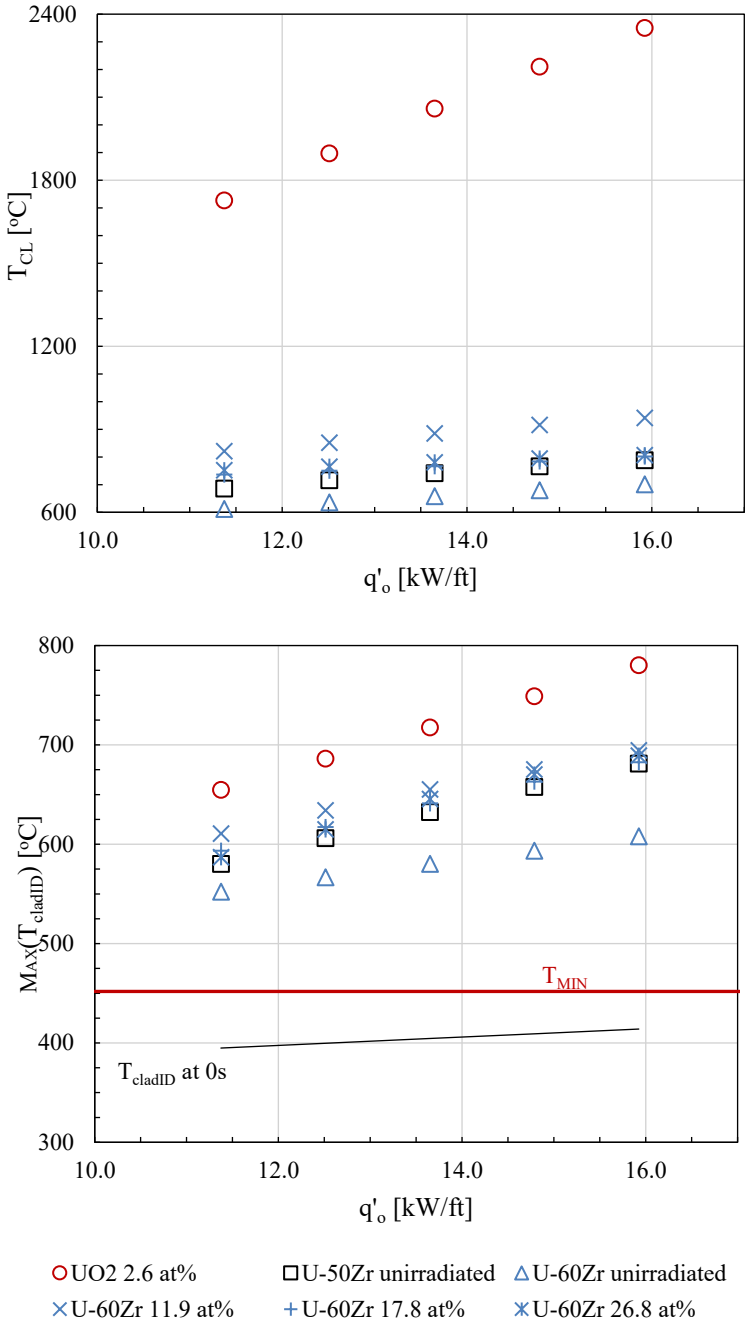

Figure 6. Fuel centerline and peak cladding temperatures.

The following key observations are made for the fuel temperatures shown in Figure 6 :

a. Overall, the cladding of bonded metallic fuel with all six U-Zr properties tested in this exercise experienced temperature increases in the range of 150 to 300°C with the peak temperature always remaining below 700°C. The peak temperatures were observed within 1 to 2 seconds after film boiling was initiated in all cases. These temperatures are well

below any known limit for Lightbridge's metallurgically bonded, monolithic U-Zr alloy fuel form, based on the operating experience and qualification data.

The fuel centerline temperatures in Figure 6 are higher than the phase transition temperature for the intermetallic δ-UZr_2 phase. With a ~300°C temperature drop from the centerline to the rod surface, only a small fraction of fuel in this cylindrical rod geometry is exposed to temperatures higher than the phase transition. While this might be a concern, it is worth noting that the icebreaker fuel experience demonstrated stable U-Zr alloy microstructures even after annealing at temperatures above the phase transition boundary for several days. Additionally, the cruciform shape of Lightbridge fuel with a central displacer, shown in Figure 1, is designed to curb the exposure to high fuel temperatures at the fuel centerline.

b. A five-fold reduction in the thermal conductivity of irradiated U-60Zr to 11.9 at% burnup produced ~90°C higher peak cladding temperature (at 15.9 kW/ft) relative to that of the unirradiated U-60Zr. This was the highest difference in peak cladding temperature among the six U-Zr alloys (unirradiated and irradiated with 50-60 wt% zirconium).

   The irradiated U-60Zr properties reported by Gaiduchenko [19, 24] indicate a recovery of the thermal conductivity with further irradiation beyond the 11.9 at% burnup (see Figure 2). This behavior with irradiation deserves attention to understand whether there is a burnup range in which the thermophysical properties experience a minimum.

c. The differences between the peak cladding temperatures of unirradiated U-50Zr and U-60Zr alloys, ranging from 30°C (at 11.4 kW/ft) to 75°C (at 15.9 kW/ft), are notable as Takahashi et al. [18] reported only minor differences in the thermal properties of U-Zr alloys in this zirconium wt% range. Therefore, the differences between the unirradiated U-Zr alloys in Figure 2 need to be understood, especially below the phase transition temperature for the intermetallic δ-UZr_2 phase, which is the temperature range which Lightbridge fuel will predominantly experience.

d. The peak linear power of 49.7 kW/m (15.14 kW/ft), listed as "for normal operation" in Table 4.1-1 of the Byron/Braidwood UFSAR [26], happens to fall between the last two power iterations shown in Figure 6, 48.5 kW/m (14.8 kW/ft) and 52.2 kW/m (15.9 kW/ft). The peak cladding temperature for UO_2 fuel at these linear power iterations is predicted to approach to 800°C, a temperature limit where oxidation-induced zircaloy cladding embrittlement becomes a concern.

e. Considering temperature drops of approximately 300°C and 1500°C for the initial linear heat rate of 37.3 kW/m (11.4 kW/ft), from the centerline to the rod surface for U-50Zr alloy and UO_2 fuel rods, respectively, the duration of film boiling heat transfer is expected to be shorter for U-50Zr alloy fuel. In addition to the initial temperatures, the thermal time constants of both fuel types are equally significant, and these can be estimated by extending the simulation beyond the initial 10 seconds shown in Figure 4. Figure 7 shows the extended simulations that cover the entire duration of film boiling heat transfer until the rod surface is no longer too hot for liquid to maintain contact ($T_w < T_{MIN}$).

   No conclusion can be drawn from Figure 7 regarding the duration of film boiling, because an accurate simulation of film boiling heat transfer conditions, both in magnitude and time duration, requires faithful modeling of assembly-wide upstream thermal and fluid flow boundary conditions. A thermal time constant, however, can be inferred from an area-

averaged transient fuel temperature (representing a drop by ~63.2% of the total change). Under film boiling heat transfer conditions, the graphically determined thermal time constant for U-50Zr alloy and UO_2 fuels is 3.8 and 10.8 seconds, respectively, in the same cylindrical rod geometry. The shorter time constant for U-50Zr alloy fuel, approximately 2.8 times that of UO_2 fuel, is the result of its lower thermal capacitance. A shorter thermal time constant is more favorable when determining a time-at-temperature envelope.

The extended simulation shown in Figure 7 suggests a brief exposure of the U-50Zr fuel in the cylindrical rod geometry to transient temperatures higher than the phase transition boundary. This very brief exposure is limited to less than 2 seconds in this particular exercise. As noted previously, while this might be a concern in more realistic simulations of Lightbridge fuel in the context of reload licensing, the observed stability of U-Zr alloy microstructures at high temperatures and the cruciform shape of Lightbridge fuel with a central displacer mitigate this concern.

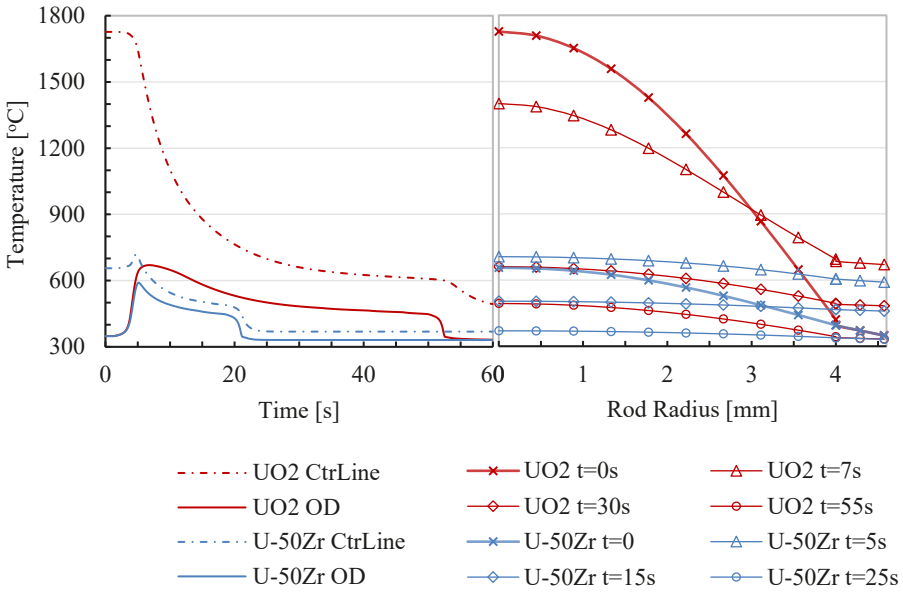

Figure 7. Transient fuel pellet and cladding temperatures.

6. CONCLUSIONS

Lightbridge fuel, with its metallurgically bonded, monolithic U-Zr alloy fuel form, has an advantage in implementing the time-at-temperature strategy, benefitting from its thermophysical properties along with a decades long maritime application experience which had demonstrated a robust performance by zirconium-rich U-Zr alloy fuels. The case studied here, the instantaneous seizure of a reactor coolant pump rotor event, shows that fuel temperatures remain well below any known limit for it (based on the operating experience and qualification data) even during one of the most challenging plant transient events. To focus on the effect of thermophysical properties, the case used Lightbridge fuel in the cylindrical geometry of a standard PWR 17x17 type fuel rod, rather than the helical cruciform shape for which Lightbridge fuel is known. By using the thermophysical properties for unirradiated and irradiated with 50-60 wt% zirconium from two different

sources, the case study also addresses a potential concern about the lack (and uncertainty) of thermophysical properties for irradiated U-Zr alloys of Lightbridge fuel.

It is also anticipated that a time vs. temperature envelope for Lightbridge fuel will be based on the material properties of the fuel core and the integrity of metallurgical bond, rather than the properties of coextruded cladding layer alone. These properties will be measured over a wide range of burnup levels anticipated for Lightbridge fuel's use in commercial LWRs. The following table, which converts the irradiated U-Zr alloy fuel burnup values to energy per unit mass (MWd/kgU), is provided as a reminder that the icebreaker fuel samples, to which the thermophysical properties used in this study belong, had achieved burnup levels nearly four times the burnup levels of typical UO_2 fuel in LWRs.

Table III. Burnup conversion for the irradiated fuel in Figure 2.

Fuel Type	MWd/kgU	at%	g/cc
UO_2	25	2.6	0.24
U-60Zr	113	11.9	0.4
U-60Zr	169	17.8	0.6
U-60Zr	255	26.8	0.9

As a final note, Lightbridge is sponsoring a fuel development program at INL that encompasses fabrication development, test sample fabrication, irradiation experiments, and associated post-irradiation examinations. The planned irradiation testing, along with post-irradiation examinations and material characterization, will generate the thermophysical properties of Lightbridge fuel. Lightbridge is also undertaking a thermal-hydraulic development program to characterize the performance of its helical cruciform fuel to support U.S. domestic PWR and BWR applications. The activities include the optimization of geometry for specific applications and future testing to support fuel licensing.

REFERENCES

[1] J. Beale and D. Schrire, "Test Matrix for Determining the Impact of Critical Heat Flux on Cladding Material Behavior," Palo Alto, CA, Dec. 2024.

[2] "NUREG-0800 United States Nuclear Regulatory Commission Standard Review Plan Office Of Nuclear Reactor Regulation," 2000.

[3] T. Hara, S. Mizokami, Y. Kudo, S. Komura, Y. Nagata, and S. Morooka, "Current Status of the Post Boiling Transition Research in Japan," *J Nucl Sci Technol*, vol. 40, no. 10, pp. 852–861, 2003, doi: 10.1080/18811248.2003.9715428.

[4] D. Gualandri, P. Skelton, and M. DeVoe, "Time-at-Temperature Operation of Light Water Reactors: Survey of Literature," Sep. 2021. [Online]. Available: www.epri.com

[5] T. A. Moreira *et al.*, "Time in DNB experimental study on Cr coated zircaloy cladding," *Appl Therm Eng*, vol. 248, Jul. 2024, doi: 10.1016/j.applthermaleng.2024.123266.

[6] S. Grae, A. Morozov, and A. Mushakov, "Thorium Fuel as a Superior Approach to Disposing Excess Weapons-Grade Plutonium in Russian VVER-1000 Reactors," *Nuclear Future*, vol. 1, no. 1, pp. 37–41, 2005.

[7] S. Holcombe, A. Mushakov, and J. Fornof, "Development Of Lightbridge's Advanced Metallic Fuel For Water-Cooled Reactors," in *Top Fuel 2024 Reactor Fuel Performance*, Grenoble, France: European Nuclear Society, Sep. 2024, pp. 259–267.

[8] V. V. Bol'shakov, S. M. Bashkirtsev, L. L. Kobzar', and A. G. Morozov, "Experimental study of burnout in channels with twisted fuel rods," *Thermal Engineering*, vol. 54, no. 5, pp. 386–389, 2007, doi: 10.1134/S0040601507050096.

[9] T. M. Conboy, "Thermal-Hydraulic Analysis of Cross-Shaped Spiral Fuel in High Power Density BWRs," Massachusetts Institute of Technology, Cambridge, 2007.

[10] T. M. Conboy, T. J. McKrell, and M. S. Kazimi, "Experimental investigation of hydraulics and lateral mixing for helical-cruciform fuel rod assemblies," *Nucl Technol*, vol. 182, no. 3, pp. 259–273, 2013, doi: 10.13182/NT12-58.

[11] M. Kinsky, H. Kim, D. W. Pyle, J. Seo, and Y. A. Hassan, "Experimental investigation of flow regime transitions and frictional pressure drop in a 9x9 helical cruciform fuel bundle," *Nuclear Engineering and Design*, vol. 438, Jul. 2025, doi: 10.1016/j.nucengdes.2025.114074.

[12] T. Cong, R. Zhang, B. Wang, Y. Xiao, and H. Gu, "Single-phase flow in helical cruciform fuel assembly with conjugate heat transfer," *Progress in Nuclear Energy*, vol. 147, May 2022, doi: 10.1016/j.pnucene.2022.104199.

[13] K. Shirvan and M. S. Kazimi, "Three dimensional considerations in thermal-hydraulics of helical cruciform fuel rods for LWR power uprates," *Nuclear Engineering and Design*, vol. 270, pp. 259–272, Apr. 2014, doi: 10.1016/j.nucengdes.2014.01.015.

[14] K. Shirvan, "Numerical investigation of the boiling crisis for helical cruciform-shaped rods at high pressures," *International Journal of Multiphase Flow*, vol. 83, pp. 51–61, Jul. 2016, doi: 10.1016/j.ijmultiphaseflow.2016.03.014.

[15] F. A. Rough, "An Evaluation of Zirconium-Uranium Alloys," Columbus, OH, Aug. 1955.

[16] L. Leibovitz, J. M. Kramer, M. C. Billone, and J. F. Koenig, "Metallic Fuels Handbook," Argonne, IL, Nov. 1985.

[17] D. E. Janney *et al.*, "Metallic Fuels Handbook, Part 1: Alloys Based on U-Zr, Pu-Zr, U-Pu, or U-Pu-Zr, Including Those with Minor Actinides (Np, Am, Cm), Rare-earth Elements (La, Ce, Pr, Nd, Gd), and Y," 2017. [Online]. Available: http://www.inl.gov

[18] Y. Takahashi, M. Yamawakl, and K. Yamamoto, "Thermophysical Properties of Uranium-Zirconium Alloys," *Journal of Nuclear Materials*, vol. 154, pp. 141–144, 1988.

[19] A. B. Gaiduchenko, "Thermophysical Properties of Irradiated Uranium-Zirconium Fuel," *Atomic Energy*, no. 104, pp. 5–10, 2008.

[20] X. Ding *et al.*, "Magnetic, transport and thermal properties of δ-phase UZr2," *Philos Mag Lett*, vol. 101, no. 1, pp. 1–11, 2021, doi: 10.1080/09500839.2020.1833375.

[21] Z. Hua *et al.*, "Intragranular thermal transport in U–50Zr," *Journal of Nuclear Materials*, vol. 534, Jun. 2020, doi: 10.1016/j.jnucmat.2020.152145.

[22] H. Ma *et al.*, "Impacts of irradiation-induced nanostructure on phonon linewidths and thermal conductivity in U-Zr alloy," *Phys Rev B*, vol. 108, no. 10, Sep. 2023, doi: 10.1103/PhysRevB.108.104318.

[23] G. L. Beausoleil *et al.*, "U-50Zr Microstructure and Property Assessment for LWR Applications," 2021. [Online]. Available: http://www.inl.gov

[24] B. H. Lee *et al.*, "Measurement of the specific heat of Zr-40 wt%U metallic fuel," *Journal of Nuclear Materials*, vol. 360, no. 3, pp. 315–320, Mar. 2007, doi: 10.1016/j.jnucmat.2006.10.023.

[25] "Byron Station, Units 1 & 2 and Braidwood Station, Units 1 & 2, Revision 19 to Updated Final Safety Analysis Report, Chapter 15.0, Accident Analyses - Redacted," Dec. 2022.

[26] "Byron/Braidwood Nuclear Stations, Updated Final Safety Analysis Report (UFSAR), Revision 15, Chapter 4 Reactor.," Dec. 2014.

[27] F. Eltawila and et al., "TRACE V5.0 THEORY MANUAL," Rockville, 2006. [Online]. Available: https://www.nrc.gov/docs/ML1200/ML120060218.pdf

[28] D. C. Groeneveld *et al.*, "The 2006 CHF look-up table," *Nuclear Engineering and Design*, vol. 237, no. 15-17 SPEC. ISS., pp. 1909–1922, Sep. 2007, doi: 10.1016/j.nucengdes.2007.02.014.

[29] T. A. Moreira *et al.*, "Time in DNB experimental study on Cr coated zircaloy cladding," *Appl Therm Eng*, vol. 248, Jul. 2024, doi: 10.1016/j.applthermaleng.2024.123266.